




Abid Hasan RAFI ¹, Mohammad Rejaul HAQUE ¹,
Dewan Hasan AHMED ¹

Two-dimensional analogies to the deformation characteristics of a falling droplet and its collision

Received 6 April 2021, Revised 11 October 2021, Accepted 21 November 2021, Published online 28 December 2021

Keywords: droplet, freefall, spreading, drag force

The present study investigates the 2D numerical analogies to the changes of the droplet shapes during the freefall for a wide range of droplet sizes through the stagnation air. The freefall velocity, shape change due to frictional force during free-fall is studied for different considered cases. With the elapse of time, a droplet with a larger initial diameter is changing its original shape more compared to droplets with a smaller diameter. In addition, the spreading of the droplet during the freefall seems more rapid for the larger-diameter droplet. When a droplet with an initial diameter of 15 mm starts to fall with gravitational force, the diameter ratio is decreasing for droplets with higher density and surface tension while droplets having lower density and surface tension show a diameter ratio greater than one. The spreading and splashing of the droplet on a solid surface and liquid storage at the time of impact are much influenced by the freefall memories of the droplet during the freefall from a certain height. These freefall memories are influenced by the fluid properties, drag force, and the freefall height. However, these freefall memories eventually regulate the deformation of the droplet during the freefall.

1. Introduction

Droplet motion and its dynamic behavior is a very interesting phenomenon in different engineering applications. Droplet dynamics and its interaction with surrounding fluids, changes of shapes during its free fall, and different fluid dynamics aspects are among the considerable issues to the researchers. The droplet

✉ Dewan Hasan AHMED e-mail: dhahmed.mpe@aust.edu

¹Department of Mechanical and Production Engineering, Ahsanullah University of Science and Technology, Dhaka, Bangladesh; ORCID: A.H.R.: 0000-0002-5518-9088; M.R.H.: 0000-0003-3105-0927; D.H.A.: 0000-0002-7024-249X



© 2022. The Author(s). This is an open-access article distributed under the terms of the Creative Commons Attribution-NonCommercial-NoDerivatives License (CC BY-NC-ND 4.0, <https://creativecommons.org/licenses/by-nc-nd/4.0/>), which permits use, distribution, and reproduction in any medium, provided that the Article is properly cited, the use is non-commercial, and no modifications or adaptations are made.

impacts on dry and wet surfaces are also concerned issues in different industrial applications like inkjet printing process [1–3], soil erosion [4–6], spray coating [7, 8], spray cooling [9–11], pesticide spraying [12, 13], and fire suppression by sprinkler system [14, 15], etc. However, most of the investigations on the droplet impact are carried out with the simplified spherical shape of the droplet. Also, the larger droplet is not in spherical shape at the time of impact when it is in free fall with an elevated velocity for any particular industrial application.

The characteristics of the free fall droplet depend on various parameters like droplet sizes, environmental conditions, fluid properties, etc. Initially, droplets tend to be spherical due to surface tension. When a droplet is falling through stagnant air, the frictional force is working against the gravitational force. Significant research works are carried out in wind tunnels by the researchers [16, 17] and mathematical models of the equilibrium shape of water droplets have been proposed by other researchers [18, 19]. It has been found that the falling droplets of size smaller than the capillary length (3 mm for water) remain quasi-spherical and droplets with large diameter are stretched along the horizontal plane creating liquid “coins” and get flattened until they burst during the freefall [20].

Clift et al. [21] stated that in the limit of large velocities, inertial friction could exceed surface forces, which leads to the deformations of the fluid globules. Yao and Schrock [22] experimentally studied droplet deformation and found that a non-spherical shape is formed during freefall for a droplet diameter larger than 4 mm. Horton et al. [23] reported that a droplet behaves like a rigid sphere during its free fall when it does not circulate. Moreover, Magarvey and Taylor [24] considered droplets ranging from 10 mm to 20 mm equivalent diameters to fall down of a 15 m stairwell for the observation of deformation and instability of large-sized droplets. Also, Chowdhury et al. [25] concluded that the falling height values of approximately 6 m and 12 m can be used as reference data to study droplet freefall. However, Abdelouhab and Gatignol [26] stated that it takes forever for a droplet to reach its terminal velocity, theoretically. Hence, it is necessary for the droplet to travel an endless distance, therefore, they concluded that free-fall velocity just reaches 95% of its terminal velocity. Boxel [27] reported that 5 m height is required for a droplet of 10 mm diameter to obtain 90% of its terminal velocity and around 6 m height is required to obtain 95% of its terminal velocity. Hence, the required height is in decreasing trend with the increment of droplet diameter. In addition, the droplet shape is changed during the free fall and its horizontal axis is increased with the elapse of time [18, 24, 28, 29]. Therefore, the axis ratio which is defined as the ratio between the minor axis and the major axis of the droplets decreases with the increase of free fall height.

According to Josserand and Thoroddsen [30], when a droplet hits on a solid surface, from smooth spreading to splashing, jetting, and rebound phenomenon of the droplet can be observed. Eggers et al. [31] mentioned that the kinetic energy of a droplet is converted into surface energy and the viscosity of fluid comes into play near the solid surface. In droplet physics, Weber number (We) and the Reynolds

number (Re) mostly determine the dynamics of droplets upon impact. The relation between kinetic and surface energy is measured by We . A droplet with a larger We acquires a larger surface area due to maximum spread. Moreover, a higher Re means the viscous effects are confined close to the solid surface. According to Chandra and Avedisian [32], when a droplet hits on a solid surface, it can splash, spread, and/or rebound. For higher impact energy as well as higher We , the droplet may burst during deformation, whereas droplets with lower We may stick to the surface and spread. Ultimately, it stays as a lens-shaped mass or rebound from the surface. Moreover, Engel [33] found that spherical drop initially deforms into a truncated sphere and later generates a circular shape. However, rebound and bounce-off phenomena weren't indicated in these experiments. Moreover, the researchers are given much concern about Re , We , and Oh numbers for droplet impact characteristics on solid surfaces. The non-dimensional numbers can be described as below:

The Weber number (We) and Reynolds number (Re) are expressed as:

$$We = \frac{\rho V^2 d}{\sigma}, \quad (1)$$

$$Re = \frac{\rho V d}{\mu}. \quad (2)$$

Here, ρ is density, V is velocity, d is diameter of the droplet, σ is surface tension, and μ is dynamic viscosity.

The Ohnesorge number (Oh) is used to relate the viscous force with surface tension force as well as it can be expressed as a function of We and Re :

$$Oh = \frac{\sqrt{We}}{Re}. \quad (3)$$

However, when a droplet starts to spread on a surface without splashing, it will continue to spread until reaching the maximum radius. Depending on the surface properties, the liquid will recede or stay close to this maximum spread [34]. For a superhydrophobic surface, a partial or full rebound can be observed and even a singular jet can be formed due to the retraction of the droplet [35–37]. According to Clanet et al. [38], when a droplet larger than capillary length begins to spread on the surface to reach its maximal deformation, it looks like a puddle. A droplet smaller than capillary length is unable to form a puddle because of the domination of surface force over gravitational force, so the drop will remain closer to a spherical shape.

Researchers [39–41] observed that a droplet splashed if the $We > 80$ and smaller droplets are generated from the primary droplet. Droplets with $30 < We < 80$ never disintegrate until it (We) begins to rise from a hot surface. For smaller $We \leq 30$, the disintegration of the droplet was not observed. Another group of researchers [42–45] concluded that normally droplets don't splash on smooth, flat, dry surfaces and splashing occurs only if the surface is rough (non-flat) or the

droplet hits on a liquid or a shallow pool. However, Stow and Hadfield [46] stated that splashing is possible on a smooth, dry surface if the droplet hits the surface with an impact velocity higher than a threshold value. With the increase of impact velocity, the droplet splashed and ejected into smaller pieces. Mundo et al. [47] proposed a splashing parameter, k_{th} to characterize the threshold value of spreading where the inertia, surface tension, and viscous stress incorporated in the form of We , and Re as well, can be expressed by Eq. (4).

$$k_{th} = We^{0.5} Re^{0.25}. \quad (4)$$

For impacts at $k_{th} \geq 57.7$, a splash can be expected, according to Bussmann et al. [48].

For droplets with a higher We , the surrounding air creates instability of the spreading droplet which makes the droplet unsteady and asymmetric. Xu et al. [49] suggested that this unsteady situation can be avoided by reducing the gas pressure about a factor of 5 below the atmospheric pressure.

Creating the perfect shape of a droplet is one of the challenging tasks to perform experimentally. According to Magarvey and Taylor [24], much difficulty came across in the production of droplets sufficiently large to observe shape changes. Different dropping techniques were used for the droplet formation, but producing a complete spherical droplet is still a challenging task. An apparatus with significant height is needed to conduct this type of experiment. Hence, computational fluid dynamics can play a vital role to study droplet dynamics.

In the field of computational studies, axisymmetric deformation of liquid droplets has been studied by [50–52]. Feng and Beard [52] showed the breakdown for larger droplets both experimentally and theoretically with axisymmetric assumption. Also, researchers [53, 54] demonstrated the breakup of liquid droplets with a constant body force and impulsive acceleration in a computational way. The unsteady Navier-Stokes equation for both the droplet and surrounding fluid is solved by using a finite-difference/front tracking numerical technique. The breakup process is controlled by the We , Re , Oh , and the Eötvös number, Eo .

The Eötvös number, (Eo) expressed below is used to compare the importance of gravitational force and surface tension force for characterizing the shape of bubbles or droplets moving through a surrounding fluid:

$$Eo = \frac{\Delta\rho g d^2}{\sigma}. \quad (5)$$

Here, $\Delta\rho$ is density difference of the two fluids, g is gravitational acceleration.

To simulate multiphase phenomena including deformation and topological change, interface tracking techniques are used because the interface evolves with the mesh. The volume of fluid (VOF), Level-set, Phase-field, Lattice Boltzmann methodologies are some from this category [55]. Sussman and Puckett [56] also developed a hybrid Level-set-VOF method to take the advantage of both Level-set and VOF methods together.

In the VOF method, the interface is reconstructed using the stored volume fraction data in each computation cell. VOF method has an excellent mass conserving property [57]. Also, topological changes during deformation or breakup are implicit in the formulation and thus the VOF method is suitable to study the droplet dynamics and breakup physics as well as it is relatively easy to use the VOF method in parallel computation, because only the neighboring cells are needed to update the volume fraction [55]. However, the work investigated the structural dynamics of the liquid droplet breakup process by using the VOF interface capturing methodology.

Numbers of numerical studies could be found in literature and compared the numerical studies on droplets in 2D, 2D axisymmetric, and 3D simulation with reasonable agreement. For example, Shin and Juric [58] reported the droplet impact on a solid surface in 2D, 2D axisymmetric, and 3D models and obtained results that were in good agreement with numerical and experimental results. Similar conclusions were drawn by García Pérez and Vakkilainen [59], Mezhericher et al. [60] for 2D, 2D axisymmetric, and 3D models for CFD analysis. Similarly, Afkhami and Bussmann [61] reported that droplet deformation in 2D simulation results show a qualitatively similar trend with experimental results where the 2D data are relatively under predicts the data and, on the other hand, experimental results are qualitatively different from 3D simulations.

Usually, the 2D model nullifies the interaction of the viscous force inside the droplet in the Z direction, hence, when it impacts on any surface, it shows lower velocity and impact force compared to a 3D model [62]. However, the overall deformation trend is very well matched with the experimental and analytical results in 2D simulation instead of the 3D model which requires a very high computational cost [62].

Therefore, the main focus of the present study is to investigate droplet dynamics during free fall for larger droplets for different conditions using a computational tool. The initial droplet diameter range is from 8 mm to 25 mm to study the shape change of the water droplet during freefall. However, the initial diameter is considered as 15 mm to investigate the shape change of droplets of different fluids during freefall. The same initial diameter is also considered for studying the impact phenomena of a particular fluid droplet on a solid surface and liquid storage or pool after the freefall. Hence, inspired by Zheng et al. [62], the present simulation studies have been done in 2D to reduce the computational cost significantly as well as with a good understanding of the problem.

2. Models and methods

2.1. Physical model

The 2D computational domain considered in the present study is a rectangular channel of 5 m height and 150 mm width where the circular droplet falls due to gravity. ANSYS Fluent software is used to investigate the freefall droplet

characteristics and its impact on the solid and liquid surface. In a very recent research, Thalackottore Jose and Dunne [63] carried out numerical simulation in ANSYS Fluent software in a 2D model to investigate the droplet impingement on a flat surface rather than a 3D model and obtained a considerable conformity with experimental results. It is reported by [62] that the overall deformation of the droplet trend is matched very well with the experimental and analytical results in 2D simulation instead of the 3D model which requires a very high computational cost. Therefore, the present numerical studies are carried out in 2D to reduce the computational cost and time significantly.

According to Boxel [27], a minimum of 5 m height is required to attain 90% of the terminal velocity of a droplet having 10 mm diameter. Therefore, in the present study, 5 m height is considered to study the dynamics of droplets having a diameter ranging from 8 mm to 25 mm. The computational domain with corresponding dimensions and meshing of the domain are shown in Fig. 1a and Fig. 1b respectively.

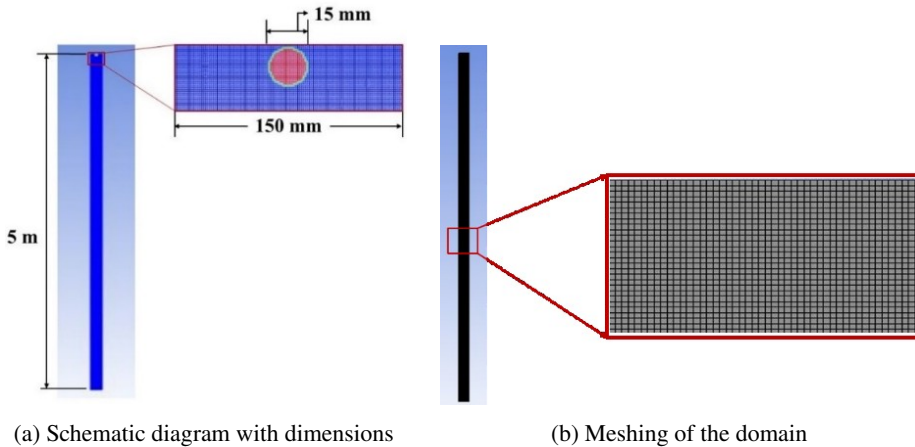


Fig. 1. The computational domain

2.2. Governing equations and boundary conditions

In developing the two-dimensional model, some assumptions are considered for the simplification of the analysis. The model is a transient state, fluid properties are constant (i.e., density, viscosity) and the flow is considered as incompressible and laminar flow. The governing equations for mass conservation and momentum conservation can be obtained from the following equations:

Continuity Equation:

$$\frac{\partial u}{\partial x} + \frac{\partial v}{\partial y} = 0. \quad (6)$$

Momentum Equations:

X-momentum:

$$\frac{\partial(\rho u)}{\partial t} + \nabla(\rho u \vec{V}) = -\frac{\partial \rho}{\partial x} + \frac{\partial \tau_{xx}}{\partial x} + \frac{\partial \tau_{yx}}{\partial y} + \rho f_x. \quad (7)$$

Y-momentum:

$$\frac{\partial(\rho v)}{\partial t} + \nabla(\rho v \vec{V}) = -\frac{\partial \rho}{\partial y} + \frac{\partial \tau_{xy}}{\partial x} + \frac{\partial \tau_{yy}}{\partial y} + \rho f_y. \quad (8)$$

When an object is falling through the surrounding air, two external forces play a major role in its dynamics. One is the gravitational force (W) and the other force is air resistance or the drag force (D). The gravitational force, W , acting on a uniform droplet can be found in Eq. (9):

$$W = \frac{1}{6} g \pi d^3 (\rho_s - \rho_a), \quad (9)$$

where: g is acceleration due to gravitational force, d is diameter of the droplet, ρ_s is density of the droplet, ρ_a is density of the surrounding fluid (air).

The drag force (D) depends on the drag co-efficient (C_D), the falling velocity (V), and the surface area (S). Equation (10) can be used to evaluate the drag force.

$$D = \frac{1}{2} \rho V^2 S C_D \quad (10)$$

The falling velocity (V) of a falling body with gravity can be obtained from:

$$V = u + gt, \quad (11)$$

where, u is initial velocity of the falling body, t is falling time.

Falling time (t) for a falling body from height (h) can be obtained from:

$$t = \sqrt{\frac{2h}{g}}. \quad (12)$$

Water tends to be drawn into a spherical shape due to the surface tension effect. All liquid droplets would be approximately spherical if only the surface tension force is working on them. If the droplet size is smaller than the capillary length, then surface tension dominates over the gravitational force. For a fluid-fluid interface, the capillary length can be obtained from:

$$\lambda_c = \sqrt{\frac{\sigma}{\Delta \rho g}}, \quad (13)$$

where, σ is surface tension of the fluid interface, $\Delta\rho$ is difference of density between fluids. If the diameter is less than the capillary length, it will follow the Stokes' law.

The surface tension in this model is used as a continuum surface force, which is coupled with a momentum equation. \vec{F}_{SA} , denoted below is a combination of normal surface force and tangential surface force.

$$\vec{F}_{SA} = \vec{F}_{SA}^n + \vec{F}_{SA}^t. \quad (14)$$

Here, \vec{F}_{SA}^n is normal surface tension force, \vec{F}_{SA}^t is tangential surface tension force. For surface tension force per unit interfacial area, the above equation changes to Eq. (15).

$$\vec{F}_{SA} = \sigma\kappa\hat{n} + \nabla_s\sigma. \quad (15)$$

Here, κ is interface curvature, ∇_s is gradient operator tangent to the interface.

The initial velocity of the droplet is 0 m/s and the gravity is set to 9.81 m/s². The pressure is atmospheric pressure, which is 101325 Pa, and the temperature of the model is 25°C. The present study is considered for different fluid properties mentioned in Table 1 to study the effect of droplet density and viscosity on droplet dynamics.

Table 1. Properties of fluids

Fluid	Density, (kg/m ³)	Viscosity, (kg/m s)	Surface tension with air, (N/m)
Diesel	730	0.0024	0.02584
Water	998.2	0.001003	0.073
Glycerin	1260	0.799	0.064
Mercury	13530	0.001523	0.4855

2.3. Volume of fluid

For the simulation, the Navier-Stokes equations are coupled with the Volume of Fluid (VOF) which is used to follow a droplet during free fall. The method is based on a concept of a scalar fraction function of liquid volume, which is represented by the fraction of liquid volume in each cell. The volume fraction of each fluid is tracked through every cell in the computational grid, while all fluids share a single set of momentum equations [55, 57, 61].

The average value of C in a cell would represent the fractional volume of the cell occupied by fluid. When a cell has no traced fluid inside, the value of C is zero and when the cell is full, the value of C is 1; and for fluid interface in the cell, the value of C is $0 < C < 1$.

The change of the w -th fluid in a system of n fluids is governed by:

$$\frac{\partial C_w}{\partial t} + v \nabla C_w = 0, \quad (16)$$

with the following constraint

$$\sum_{w=1}^n C_w = 1.$$

A pressure-based solver is used, in which velocity formulation is absolute. For the multiphase model, the viscous model is used as a laminar in which the number of Eulerian phases is 2, and the volume fraction formulation is implicit.

2.4. Numerical method

The discretization process is done with the finite volume method to solve the partial differential equations i.e., Navier-Stokes equations where the computational domain is discretized into a series of finite volumes or cells. Within the problem domain, the physical parameters are represented as discrete nodes surrounded by finite volumes. The volume integrals with a divergence term are substituted by surface integrals using the divergence theorem. For phase interaction, the continuum surface force model is used and the algorithm SIMPLE (semi-implicit method for pressure-linked equations) is used for pressure-velocity coupling. The least squares cell-based method is considered to achieve sufficient accuracy and also to minimize the computational time and in addition, the implicit body force treatment is also applied to improve the solution convergence. Time step size is 0.0002 s and the model runs for numbers of iterations till the convergence is achieved for at least 3 orders for all the converging parameters. The computational cost for performing a single simulation case was approximately 2.5–3 hours on an 8.00 GB RAM, Intel(R) Core(TM) i3-8100 CPU @ 3.60 GHz.

2.5. Mesh generation and grid independence test

Meshing is one of the important parts of simulation as the calculated result's accuracy significantly depends on meshing elements. For the present study, the Quadrilateral Dominant method is used to mesh the entire domain (Fig. 1a). The element order is linear and the element size is 0.00125 m. The maximum layers, growth rate, and inflation are 0.272, 2, and 1.2 respectively. The meshing of the domain is shown in Fig. 1b.

A grid independence test is also performed to reduce the influence of the number of grid sizes on the computational results. During the test, a sequence of coarse, medium, and fine meshes are generated to observe the effect on a specific parameter such as the magnitude of velocity.

For the grid independence test, a droplet was set on this domain at 0.5 m height from the surface. Velocity magnitude was calculated for six different element sizes of the grid, as shown in Fig. 2, where s is the element size of a single grid. Meshing with grid size $s = 0.003$ m is considered as coarse meshing while s decreases up to 0.001 to check the effect of grid size. Therefore, six different (0.003 m, 0.002 m, 0.00175 m, 0.0015 m, 0.00125 m, and 0.001 m) mesh sizes were considered for

the tests. From Fig. 2, it is shown that there are little fluctuations in the velocity magnitude as time varies from $t = 0.2$ s to 0.3 s. The maximum deviation of the velocity is observed to be less than 4% due to the changing of grid sizes from coarse to fine. Therefore, for the present study, 0.00125 m grid size is considered. Hence, for this grid size, the total number of nodes is 484114 with the number of elements is 479995.

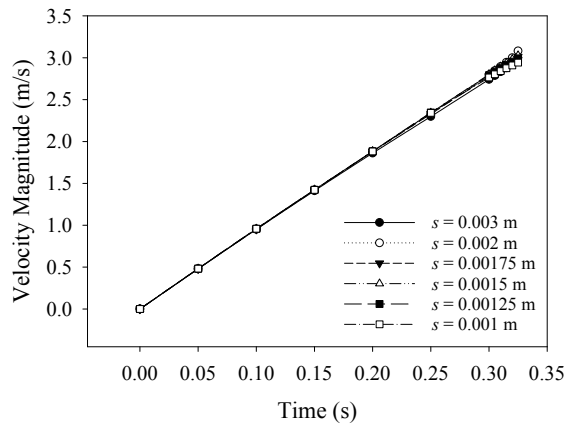


Fig. 2. Grid independence test

2.6. Validation

When a droplet is falling through stagnant air, its shape changes due to friction with the surrounding fluid where shape changes are much influenced by the size of the droplets. Fig. 3 shows the contour of water volume fraction of droplet for the droplet sizes (8, 10, 15, 20, and 25 mm). It is clearly evident from the figure that droplets are much stretched in the horizontal direction and it is much more for the case of the larger droplets. It should be noted here that the liquid fraction shown in Fig. 3 is just before the droplets breaking down to multiple droplets.

For the validation purpose, the axis ratios (droplet's vertical to horizontal dimension) of different droplet diameters (8 mm to 25 mm) are plotted and compared with the available literature [24] as shown in Fig. 4. The displayed axis ratio in Fig. 4 is calculated from the droplet shape just before it breaks into multiple droplets. As it is expected, the droplets are stretching in the horizontal direction and the larger droplets are much stretched as compared to smaller droplets, and the axis ratio becomes smaller for the larger droplets. From Fig. 4, it is observed that the values of the axis ratio computed in the present study follow a similar trend to the results of earlier works.

The falling velocity of a water droplet with time for different diameters ranging from 8 mm to 25 mm is calculated numerically and compared with the analytical value by Eq. (11) is shown in Fig. 5a. The velocity of droplets, just before a droplet

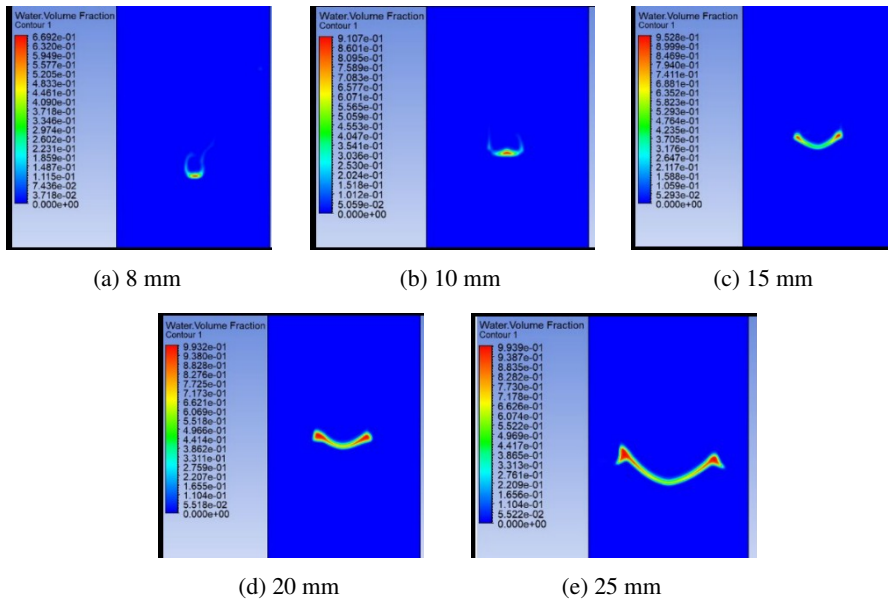


Fig. 3. Surface plot of water volume fraction of droplets having various diameters

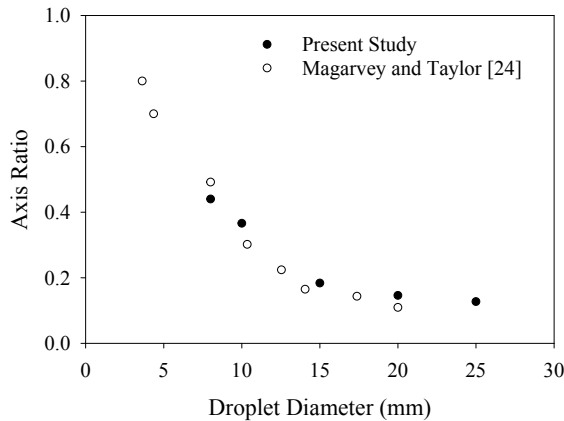


Fig. 4. Axis ratio as a function of droplet diameter

breaks down into multiple droplets, for different droplet sizes is shown in Fig. 5b. It could be stated that the larger droplets have higher velocities as compared with the smaller droplets as the gravitational force is much higher than the drag forces at the initial stages. However, as time goes on, the drag force is increased, therefore, the increment of the velocities of the smaller droplets is gradually diminishing earlier. On the other hand, drag forces make an unstable condition for the larger droplets and result in changes of the shape of the droplets as the pressure at the upstream position of the droplet becomes larger (stagnation point), allowing the fluid flow

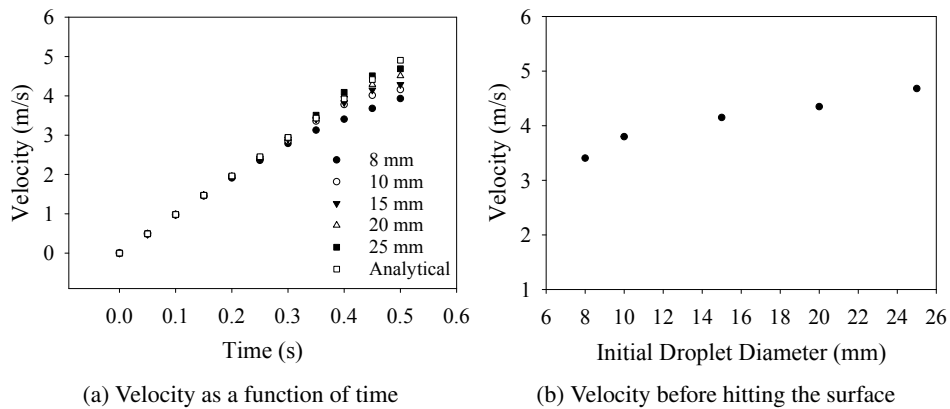


Fig. 5. Velocity of water droplets

in the peripheral direction (as evident in Fig. 3) and a droplet breaks into smaller droplets.

As a droplet moves with a velocity relative to the ambient, it is acted upon by aerodynamic drag force. The drag force, in turn, creates differential pressure distribution around the droplet and causes it to deform. The other forces acting on the droplet are the surface tension force and the skin friction force (internal and external) due to the droplet and air viscosity. With the elapse of time, the droplet starts to break after significant deformation. Therefore, it can be concluded that the presented numerical results are quite comparable with the available literature results as shown in Figs. 3–5.

3. Results and discussion

3.1. Effect of the initial diameter of a water droplet on the droplet shape change

Shape changes of water droplets are calculated numerically for the droplet diameters range of 8–25 mm. Droplet diameter larger than 5 mm is unstable, and the droplet starts to break after a certain time of fall [20, 24]. Therefore, for droplet diameter larger than 5 mm, the difference in shape change is evident because of its instability. Due to free fall from an initial height with zero velocity, the change of diameter is negligible for a certain initial period. At $t = 0$ s, the droplet is circularly shaped. When it starts to fall, the circle is turning into a flat shape and expands in the horizontal direction at around $t = 0.3$ s for all five different diameters of droplets, as shown in Fig. 6. The larger the initial diameter of the droplet, the faster the shape change takes place.

After that, the diameter in the horizontal axis increases as the droplet continues to fall. Droplet size with larger diameter experiences more frictional resistance and spreads in the horizontal direction more rapidly. The horizontal diameter is denoted

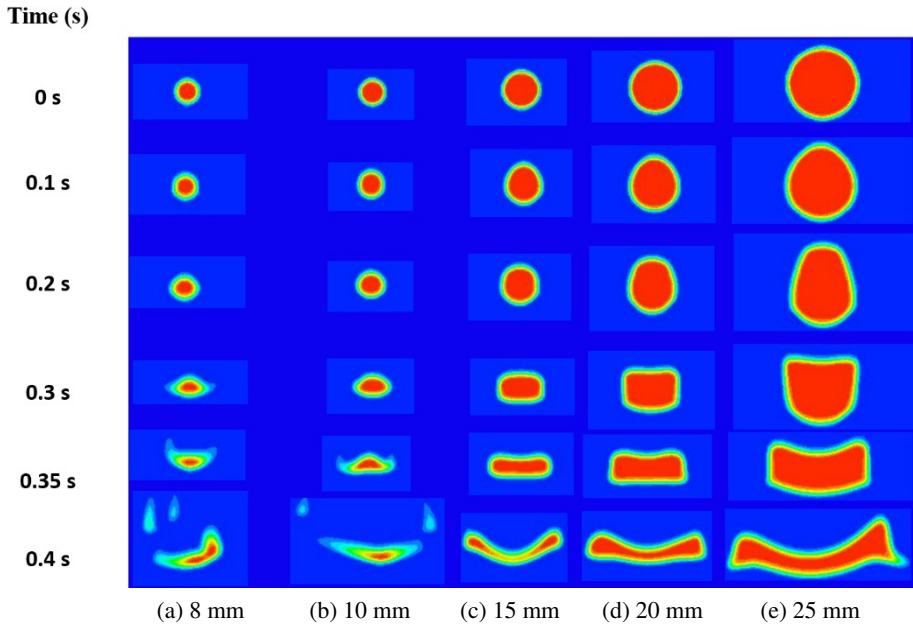


Fig. 6. Shape change of water droplet with various initial diameters (D)

as D_H and the initial diameter as D . The ratio of horizontal diameter to initial diameter (D_H/D) and vertical diameter to initial diameter (D_V/D) are plotted with time as shown in Fig. 7.

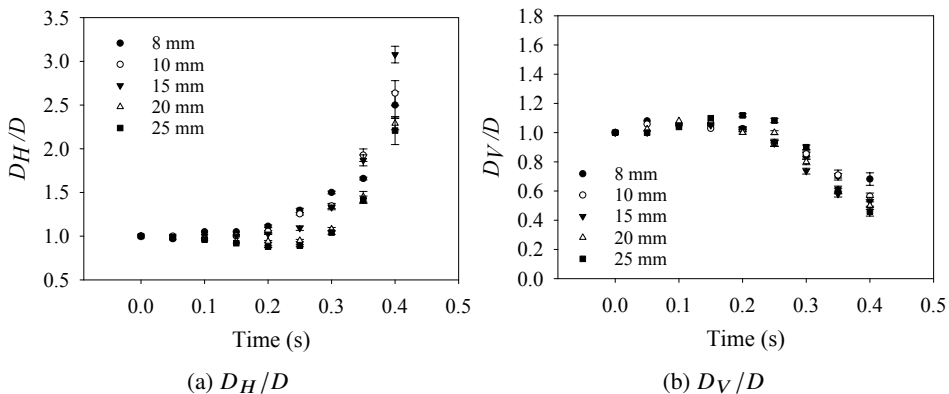


Fig. 7. The ratio of horizontal and vertical diameter to initial diameter as a function of time for various diameters of droplets

From Fig. 7a, it is observed that a droplet having a higher initial diameter has a steeper change in horizontal diameter with respect to time. It is quite interesting to observe the shape changes in the horizontal direction for the droplet with a larger diameter. Hence, the deformation in the vertical direction is more significant.

However, the confidence interval, as shown in Fig. 7, reveals that the deformation of the droplet is quite significant in both horizontal and vertical direction as time goes on, the droplet stretching in one direction leads to squeezing in the other direction. The 3D model and the experimental results might bring a better picture regarding these deformations. However, for the larger-sized droplet, the surface area in contact with the air increases more as the droplet falls through the air. Hence, the upstream face of the droplet experiences higher pressure as compared to the downstream region as it is falling down. Therefore, this relative higher pressure overcomes the surface tension forces in the upstream portion of the droplet and pushes the droplets to the downstream region through the edges as observed from Fig. 6 where the larger droplet turns into a vortex-like shape during the free fall.

3.2. Effect of liquid properties on droplet's shape

However, density is not the only factor to describe the falling dynamics, as other fluid properties may contribute to the change of droplet shape during the free fall. From Fig. 8, it is seen that the diesel droplet is spreading more compared to other liquids. The probable reason may be that both the density and surface tension of the diesel droplet is lower than that of the water droplet. Hence, for the same time-lapsed, the droplet shape of diesel is changing more abruptly compared to the water droplet. The surface tension of the glycerin droplet is slightly lower than the water droplet, but glycerin has a higher density than water causing a bell-shaped droplet with less horizontal spreading compared to both diesel and water droplets.

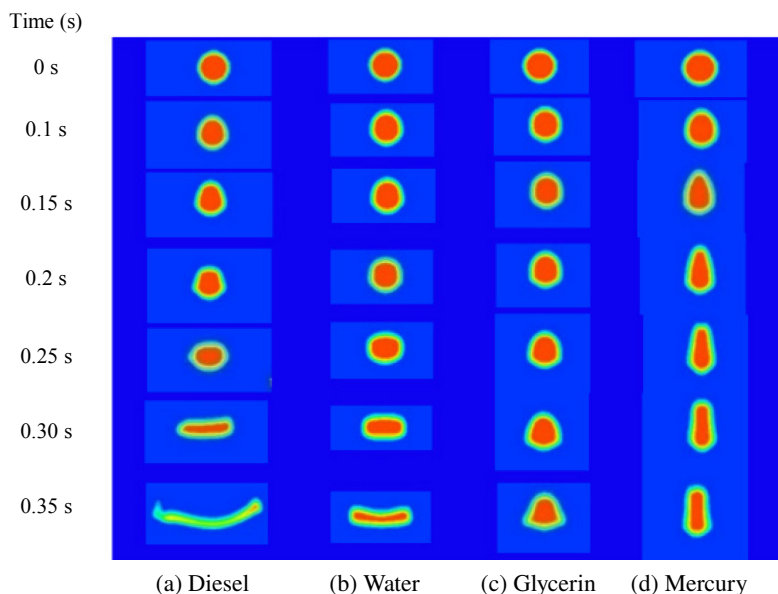


Fig. 8. Time-lapsed droplet dynamics for various liquid droplets

However, mercury has a very high density and surface tension compared to all other considered fluids that deform the droplet almost vertically, whereas both diesel droplet and water droplet are stretching almost horizontally. Hence, not only droplet density but also the surface tension force is playing a very crucial role in droplet deformation. It can be noted from the present analysis that, the higher the density of the liquid droplet, the deformation of the droplet shifts more towards the vertical direction i.e., along the flow direction.

The present study considers the horizontal diameter (D_H) and vertical diameter (D_V) measurements to elucidate the droplet deformation pattern. Both D_H and D_V are equal when a droplet is at its initial position before free falling. However, as soon as the droplet starts to fall, the diameters in both horizontal and vertical directions are changing. As already depicted in Fig. 8, the diameter change in both directions is not the same, therefore, to quantify the change, the ratio of horizontal diameter to vertical diameter, D_H/D_V is defined as the diameter ratio. In Fig. 9, the diameter ratio for different liquid droplets is shown up to the same time-lapsed.

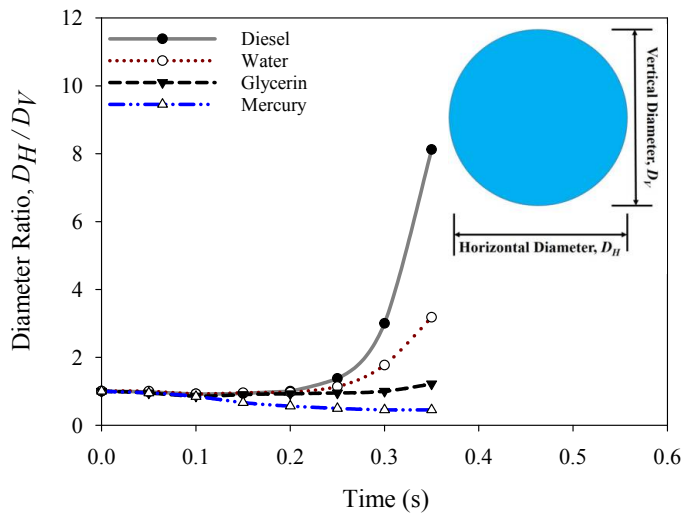


Fig. 9. For the same time-lapsed, diameter ratio of different droplets as a function of time

It is observed from Fig. 9 that the fluid with lower density starts to elongate in the horizontal direction earlier. The glycerin droplet doesn't elongate in the horizontal direction as much as diesel and water droplets. It tends to be bell-shaped later. On the other hand, the droplet of mercury shrinks in the horizontal direction. Hence, for the heavier liquid (glycerin and mercury), the droplet ratio (D_H/D_V) is found to be < 2 for the observed time-lapsed. However, for the lighter fluid (Diesel and water), the diameter ratio suddenly changes at $t = 0.25$ s, increasing to a diameter ratio of $D_H/D_V > 3$ for the observed time-lapsed. It indicates higher horizontal elongation of the corresponding droplets compared to the vertical direction.

3.3. Effect of droplet fall on a solid surface at various h/H

The present study investigates the droplet's falling time to reach a defined solid surface from different falling heights represented as h . A droplet having an initial diameter of 15 mm is placed at different falling heights. Later, falling height is calculated for different h/H ratios, where H is the height when the droplet achieves its maximum spread during free fall and h is the variable falling height of the droplet. Hence, the value of h/H varies from 0.25 to 1.0. The numerical results are compared with the analytical data obtained from Eq. (12) and the results are in good agreement. From Fig. 10, it is observed that falling time is increasing with the increase of falling height. As falling height increases, the frictional drag force acting on the droplet increases enhancing the falling time.

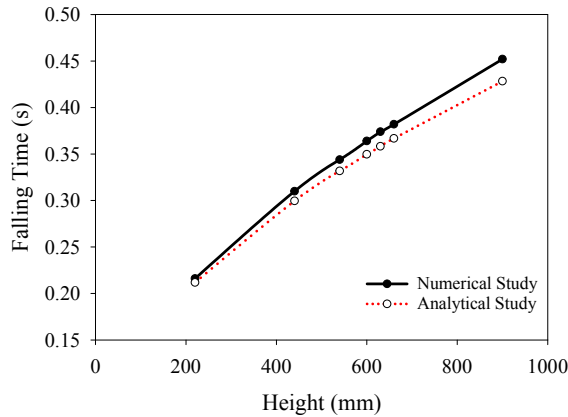


Fig. 10. Falling time to reach the surface as a function of falling height

From Fig. 11, the impact of a free fall droplet on a solid surface was observed at different $h/H = 0.25, 0.5, 0.60, 0.75,$ and 1. The considered diameter of the water droplet is 15 mm for all the cases to show the effect of h/H only. In fact, Fig. 11 shows some important insight into droplet dynamics especially when the droplet is touching on the solid surface. Spreading and splashing are clearly visible on the solid surface which is influenced by the falling height of the droplet. Other parameters, such as droplet shape and the velocity of the droplet just before the impact on the solid surface, may play a significant role in spreading and splashing on the solid surface. However, to get a better insight, the We number and other issues are needed to be considered.

According to Wachters et al. [39], a droplet with a We number higher than 80 will splash when it hits the surface. When $h/H = 0.25$, the We number is higher than 80 as well as the splashing parameter, k_{th} is also larger than 57.7. Hence, at $h/H = 0.25$, as soon as the droplet touched the surface, it turned into a truncated sphere and started to splash. After the splash, there was no rebound or jetting but it formed into a puddle structure at $h/H = 0.60$, as shown in Fig. 11, stated by Clanet

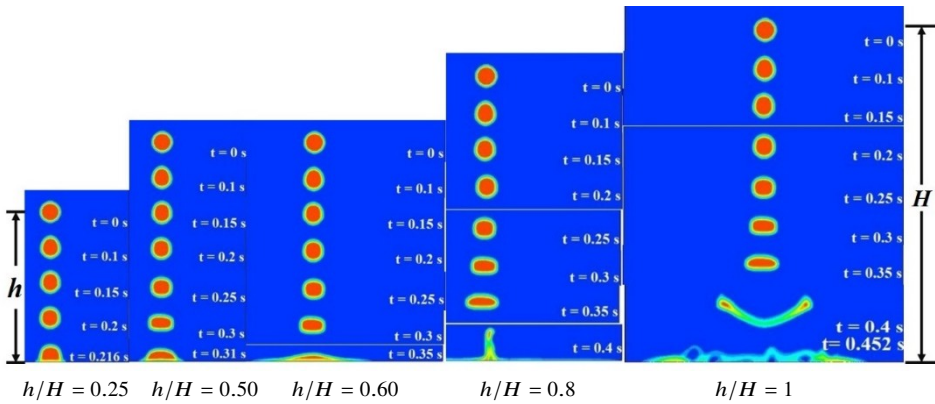


Fig. 11. Droplet falling on a solid surface

et al. [38]. The area of the puddle is increasing with the gradual increment of falling height, as shown in Fig. 12. When a droplet impacts on a surface, the kinetic energy changes into surface energy, and a droplet with a larger impact velocity overcomes the viscous effect resulting in a splash with a larger area. This phenomenon is observed until $h/H = 0.75$. However, at $h/H = 0.75$, the droplet crashes on the surface and breaks into multiple secondary droplets. One of the major reasons for secondary droplets creation is the impact and bounce off the surface. Moreover, at $h/H = 1$, multiple major secondary droplets have been created during the impact. As the droplet has a higher We number, the droplet deforms during the free fall and the impact area is larger than the initial area of the droplet. Liu [64] provided a We – Oh map to measure the effect of the impact of a droplet on a solid surface provided in Fig. 12a. The height ratio, h/H , ranging from 0.25 to 1 belongs to the splashing zone in that map which is very similar to the present results. Moreover, the splashing parameter, k_{th} calculated from Eq. (4) is shown in Fig. 12b.

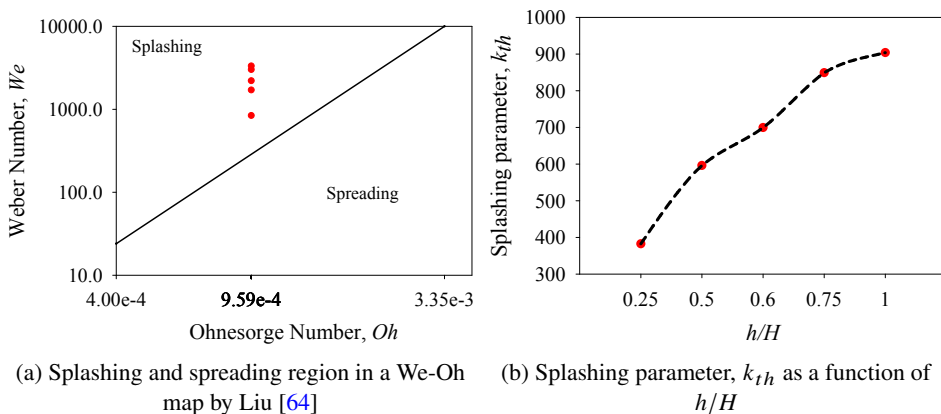
(a) Splashing and spreading region in a We – Oh map by Liu [64](b) Splashing parameter, k_{th} as a function of h/H

Fig. 12. Droplet impact characteristics on a solid surface for different free falling heights

3.4. Effect of droplet properties for falling on a Liquid Storage

To illustrate this case, droplets having an initial diameter of 15 mm for three different cases (liquids- water, glycerin, and mercury) were considered. The height (50 mm) of the liquid storage is kept the same for all cases. For all the cases, the droplet trajectories up to a time of 0.5 seconds are shown in Fig. 13, i.e., till the impact on the liquid storages. However, after the impact of the liquid droplet to the corresponding liquid storage, the scenario is quite different as droplets attain different shapes for all cases before the impact. For the case of a water droplet in Fig. 13a, it spreads much and the impact covers the larger surface of the liquid storage, while in Fig. 13c, the mercury droplet shrank before impacting the liquid storage. Moreover, at $t = 0.5$ s, the momentum of the droplet during impact makes a relatively higher disturbance in the liquid storage for the denser fluid (mercury) as compared to lighter fluid (water), as shown in Fig. 13.

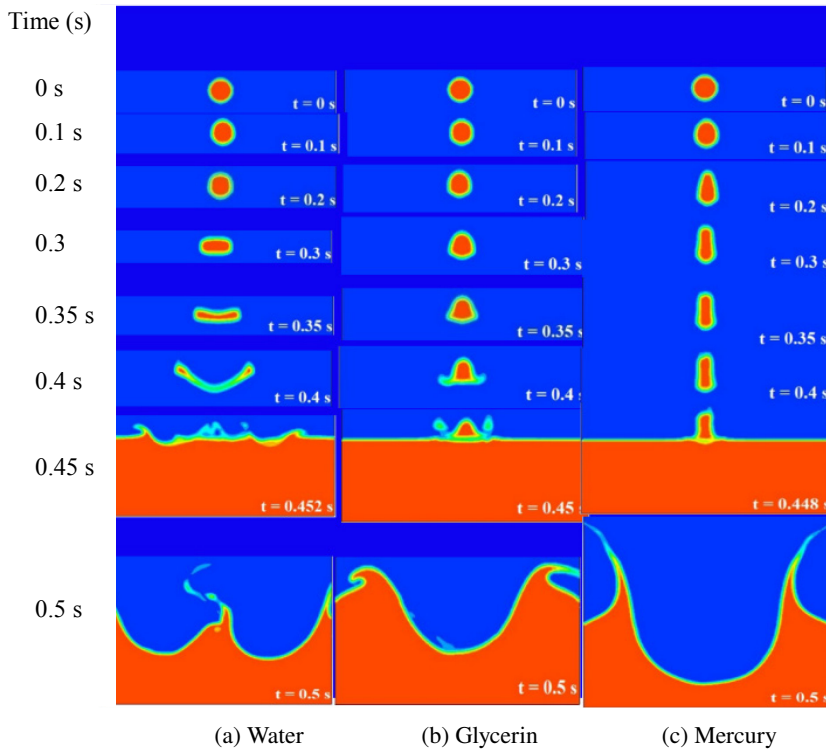


Fig. 13. Time-lapsed images of a liquid droplet falling on a reservoir of the same liquid

From Fig. 13, it is clearly seen that the crater depth increases for the denser fluid in the liquid storage (pool), however, the splashing in the liquid storage is much influenced by the free-fall memory of the droplet and its shape before impact during

the free fall. Hence, the droplet's characteristics, which are regulated by density, surface tension, height, and final shape of the droplet just before the impact, indicate the deciding factors for splashing criteria into liquid storage or the liquid pool.

4. Conclusions and recommendations

4.1. Conclusions

Droplet characteristics have several difficulties to study experimentally as the creation of different sized spherical droplets is challenging. Hence, a numerical investigation is conducted to study the effect of droplet properties and size on droplet deformation during freefall. The present simulations are carried out in a 2D model with a droplet size ranging from 8 mm to 25 mm. Even though it is difficult to produce spherical droplets in the laboratory in different dimensions, the present numerical studies are intended to investigate two-dimensional analogies to the changes of the droplet shapes during the free fall with a wide range of droplet sizes. The present simulation results are well validated with respect to the experimental and 2D results available in the literature. In a freefall droplet, friction with surrounding air plays a significant role in determining the droplet's final shape. When frictional force is greater than the surface tension force, the droplet continuously deforms and its shape is changing and the resulting diameter ratio is not equal to 1. It is found that the droplet could be deformed horizontally up to 3 times of its original dimension before impacting on the solid surface. Hence, this deformation is greatly influenced by the droplet size, density, and surface tension. Moreover, the diameter ratio is increasing at a higher rate for a droplet with a larger diameter and lower density compared to one that has a higher density. The present study also indicates that the droplet spreading or splashing on the solid surface or liquid storage is very much influenced by the falling height and the attained shape of the droplet before the impact. Moreover, the deformed shape of the droplet from its original spherical shape influences the spreading and splashing phenomena during the impact time. To conclude, the deformation of the freefall droplet is a continuous process and in addition, the spreading and splashing on a surface are much influenced by the shape of the droplet at the time of impact where the deformation of the droplet is significantly dependent on the density of the fluid and the freefall height.

4.2. Recommendations

The numerical study of the droplet in 2D, 2D axisymmetric, and 3D on freefall droplet may give a better understanding in terms of the droplet deformation during its freefall. Moreover, the computational aspects of droplet deformation need comprehensive investigation to have a clear picture of the droplet characteristics during freefall and impact on solid or liquid surfaces.

Acknowledgements

This work was supported by the Department of Mechanical and Production Engineering (MPE), Ahsanullah University of Science and Technology (AUST).

References

- [1] X. Cao, Y. Ye, Q. Tang, E. Chen, Z. Jiang, J. Pan, and T. Guo. Numerical analysis of droplets from multinozzle inkjet printing. *The Journal of Physical Chemistry Letters*, 11(19):8442–8450, 2020. doi: [10.1021/acs.jpcclett.0c02250](https://doi.org/10.1021/acs.jpcclett.0c02250).
- [2] H. Wijshoff. Drop dynamics in the inkjet printing process. *Current Opinion in Colloid & Interface Science*, 36:20–27, 2018. doi: [10.1016/j.cocis.2017.11.004](https://doi.org/10.1016/j.cocis.2017.11.004).
- [3] W. Zhou, D. Loney, A.G. Fedorov, F.L. Degertekin, and D.W. Rosen. Shape evolution of droplet impingement dynamics in ink-jet manufacturing. *Proceedings for the 2011 International Solid Freeform Fabrication Symposium*, pages 309–325, Austin, USA, 2011. doi: [10.26153/tsw/15297](https://doi.org/10.26153/tsw/15297).
- [4] L. Mouzai and M. Bouhadef. Water drop erosivity: Effects on soil splash. *Journal of Hydraulic Research*, 41(1):61–68, 2003. doi: [10.1080/00221680309499929](https://doi.org/10.1080/00221680309499929).
- [5] M. Hajjizadeh, A.M. Melesse, and H.R. Fuentes. Raindrop-induced erosion and sediment transport modelling in shallow waters: A review. *Journal of Soil and Water Science*, 1(1):15–25, 2018. doi: [10.36959/624/427](https://doi.org/10.36959/624/427).
- [6] P.C. Ekern. Raindrop impact as the force initiating soil erosion. *Soil Science Society of America Journal*, 15(C):7–10, 1951. doi: [10.2136/sssaj1951.036159950015000C0002x](https://doi.org/10.2136/sssaj1951.036159950015000C0002x).
- [7] R. Andrade, O. Skurtys, and F. Osorio. Drop impact behavior on food using spray coating: Fundamentals and applications. *Food Research International*, 54(1):397–405, 2013. doi: [10.1016/j.foodres.2013.07.042](https://doi.org/10.1016/j.foodres.2013.07.042).
- [8] M. Toivakka. Numerical investigation of droplet impact spreading in spray coating of paper. *Proceedings of the 2003 Spring Advanced Coating Fundamentals Symposium*, Atlanta, USA, 2003.
- [9] A. Prasad and H. Henein. Droplet cooling in atomization sprays. *Journal of Materials Science*, 43(17):5930–5941, 2008. doi: [10.1007/s10853-008-2860-2](https://doi.org/10.1007/s10853-008-2860-2).
- [10] W. Jia and H.-H. Qiu. Experimental investigation of droplet dynamics and heat transfer in spray cooling. *Experimental Thermal and Fluid Science*, 27(7):829–838, 2003. doi: [10.1016/S0894-1777\(03\)00015-3](https://doi.org/10.1016/S0894-1777(03)00015-3).
- [11] G. Duursma, K. Sefiane, and A. Kennedy. Experimental studies of nanofluid droplets in spray cooling. *Heat Transfer Engineering*, 30(13):1108–1120, 2009. doi: [10.1080/01457630902922467](https://doi.org/10.1080/01457630902922467).
- [12] W.-C. Qin, B.-J. Qiu, X.-Yu Xue, C. Chen, Z.-F. Xu, and Q.-Q. Zhou. Droplet deposition and control effect of insecticides sprayed with an unmanned aerial vehicle against plant hoppers. *Crop Protection*, 85:79–88, 2016. doi: [10.1016/j.cropro.2016.03.018](https://doi.org/10.1016/j.cropro.2016.03.018).
- [13] S. Chen, Y. Lan, Z. Zhou, F. Ouyang, G. Wang, X. Huang, X. Deng, and S. Cheng. Effect of droplet size parameters on droplet deposition and drift of aerial spraying by using plant protection UAV. *Agronomy*, 10(2):195, 2020. doi: [10.3390/agronomy10020195](https://doi.org/10.3390/agronomy10020195).
- [14] D.T. Sheppard. *Spray Characteristics of Fire Sprinklers*. Ph.D. Thesis, Northwestern University, Evanston, USA, June 2002.
- [15] H. Liu, C. Wang, I.M. De Cachinho Cordeiro, A.C.Y. Yuen, Q. Chen, Q.N. Chan, S. Kook, and G.H. Yeoh. Critical assessment on operating water droplet sizes for fire sprinkler and water mist systems. *Journal of Building Engineering*, 28:100999, 2020. doi: [10.1016/j.jobbe.2019.100999](https://doi.org/10.1016/j.jobbe.2019.100999).

- [16] D.C. Blanchard. The behavior of water drops at terminal velocity in air. *Eos, Transactions American Geophysical Union*, 31(6):836–842, 1950. doi: [10.1029/TR031i006p00836](https://doi.org/10.1029/TR031i006p00836).
- [17] H.R. Pruppacher and K.V. Beard. A wind tunnel investigation of the internal circulation and shape of water drops falling at terminal velocity in air. *Quarterly Journal of the Royal Meteorological Society*, 96(408):247–256, 1970. doi: [10.1002/qj.49709640807](https://doi.org/10.1002/qj.49709640807).
- [18] H.R. Pruppacher and R.L. Pitter. A semi-empirical determination of the shape of cloud and rain drops. *Journal of the Atmospheric Sciences*, 28(1):86–94, 1971. doi: [10.1175/1520-0469\(1971\)028<0086:ASEDOT>2.0.CO;2](https://doi.org/10.1175/1520-0469(1971)028<0086:ASEDOT>2.0.CO;2).
- [19] K.V. Beard and C. Chuang. A new model for the equilibrium shape of raindrops. *Journal of the Atmospheric Sciences*, 44(11):1509–1524, Jun. 1987. doi: [10.1175/1520-0469\(1987\)044<1509:ANMFTE>2.0.CO;2](https://doi.org/10.1175/1520-0469(1987)044<1509:ANMFTE>2.0.CO;2).
- [20] É. Reyssat, F. Chevy, A.L. Bianco, L. Petitjean, and D. Quéré. Shape and instability of free-falling liquid globules. *Europhysics Letters*, 80(3):34005, 2007. doi: [10.1209/0295-5075/80/34005](https://doi.org/10.1209/0295-5075/80/34005).
- [21] R. Clift, J.R. Grace, and M.E. Weber. *Bubbles, Drops and Particles*. Academic Press, 1978.
- [22] S.-C. Yao and V.E. Schrock. Heat and mass transfer from freely falling drops. *Journal of Heat Transfer*, 98(1):120–126, 1976. doi: [10.1115/1.3450453](https://doi.org/10.1115/1.3450453).
- [23] T.J. Horton, T.R. Fritsch, and R.C. Kintner. Experimental determination of circulation velocities inside drops. *The Canadian Journal of Chemical Engineering*, 43(3):143–146, 1965. doi: [10.1002/cjce.5450430309](https://doi.org/10.1002/cjce.5450430309).
- [24] R.H. Magarvey and B.W. Taylor. Free fall breakup of large drops. *Journal of Applied Physics*, 27(10):1129–1135, 1956. doi: [10.1063/1.1722216](https://doi.org/10.1063/1.1722216).
- [25] M.N. Chowdhury, F.Y. Testik, M.C. Hornack, and A.A. Khan. Free fall of water drops in laboratory rainfall simulations. *Atmospheric Research*, 168:158–168, 2016. doi: [10.1016/j.atmosres.2015.08.024](https://doi.org/10.1016/j.atmosres.2015.08.024).
- [26] M. Abdelouahab and R. Gatignol. Study of falling water drop in stagnant air. *European Journal of Mechanics - B/Fluids*, 60:82–89, 2016. doi: [10.1016/j.euromechflu.2016.07.007](https://doi.org/10.1016/j.euromechflu.2016.07.007).
- [27] J.H. van Boxel. Numerical model for the fall speed of raindrops in a rainfall simulator. *I.C.E Special Report*, 1998/1, 77–85,
- [28] A.K. Kamra and D.V. Ahire. Wind-tunnel studies of the shape of charged and uncharged water drops in the absence or presence of an electric field. *Atmospheric Research*, 23(2):117–134, 1989. doi: [10.1016/0169-8095\(89\)90003-3](https://doi.org/10.1016/0169-8095(89)90003-3).
- [29] M. Thurai and V.N. Bringi. Drop axis ratios from a 2D video disdrometer. *Journal of Atmospheric and Oceanic Technology*, 22(7):966–978, 2005. doi: [10.1175/JTECH1767.1](https://doi.org/10.1175/JTECH1767.1).
- [30] C. Josserand and S.T. Thoroddsen. drop impact on a solid surface. *Annual Review of Fluid Mechanics*, 48:365–391, 2016. doi: [10.1146/annurev-fluid-122414-034401](https://doi.org/10.1146/annurev-fluid-122414-034401).
- [31] J. Eggers, M.A. Fontelos, C. Josserand, and S. Zaleski. Drop dynamics after impact on a solid wall: Theory and simulations. *Physics of Fluids*, 22(6):062101, 2010. doi: [10.1063/1.3432498](https://doi.org/10.1063/1.3432498).
- [32] S. Chandra and C.T. Avedisian. On the collision of a droplet with a solid surface. *Proceedings of the Royal Society A: Mathematical, Physical and Engineering Sciences*, 432(1884):13–41, 1991. doi: [10.1098/rspa.1991.0002](https://doi.org/10.1098/rspa.1991.0002).
- [33] O.G. Engel. Waterdrop collisions with solid surfaces. *Journal of Research of the National Bureau of Standards*, 54(5):281–298, 1955. doi: [10.6028/jres.054.033](https://doi.org/10.6028/jres.054.033).
- [34] I.V. Roisman, R. Rioboo, and C. Tropea. Normal impact of a liquid drop on a dry surface: model for spreading and receding. *Proceedings of the Royal Society A: Mathematical, Physical and Engineering Sciences*, 458(2022):1411–1430, 2002. doi: [10.1098/rspa.2001.0923](https://doi.org/10.1098/rspa.2001.0923).
- [35] Y. Renardy, S. Popinet, L. Duchemin, M. Renardy, S. Zaleski, C. Josserand, M.A. Drumright-Carke, D. Richard, C. Clanet, and D. Quéré. Pyramidal and toroidal water drops after impact on a solid surface. *Journal of Fluid Mechanics*, 484:69–83, 2003. doi: [10.1017/S0022112003004142](https://doi.org/10.1017/S0022112003004142).

- [36] D. Bartolo, F. Bouamrine, É. Verneuil, A. Buguin, P. Silberzan, and S. Moulinet. Bouncing or sticky droplets: Impalement transitions on superhydrophobic micropatterned surfaces. *Europhysics Letters*, 74(2):299–305, 2006. doi: [10.1209/epl/i2005-10522-3](https://doi.org/10.1209/epl/i2005-10522-3).
- [37] D. Bartolo, C. Josserand, and D. Bonn. Singular jets and bubbles in drop impact. *Physical Review Letters*, 96:124501, 2006. doi: [10.1103/PhysRevLett.96.124501](https://doi.org/10.1103/PhysRevLett.96.124501).
- [38] C. Clanet, C. Béguin, D. Richard, and D. Quéré. Maximal deformation of an impacting drop. *Journal of Fluid Mechanics*, 517:199–208, 2004. doi: [10.1017/S0022112004000904](https://doi.org/10.1017/S0022112004000904).
- [39] L.H.J. Wachters, L. Smulders, J.R. Vermeulen, and H.C. Kleiweg. The heat transfer from a hot wall to impinging mist droplets in the spheroidal state. *Chemical Engineering Science*, 21(12):1047–1056, 1966. doi: [10.1016/0009-2509\(66\)85042-X](https://doi.org/10.1016/0009-2509(66)85042-X).
- [40] C.O. Pedersen. An experimental study of the dynamic behavior and heat transfer characteristics of water droplets impinging upon a heated surface. *International Journal of Heat and Mass Transfer*, 13(2):369–381, 1970. doi: [10.1016/0017-9310\(70\)90113-4](https://doi.org/10.1016/0017-9310(70)90113-4).
- [41] M.A. Styricovich, Y.V. Baryshev, G.V. TokiWauri and M E. Grigorieva. The mechanism of heat and mass transfer between a water drop and a heated surface. *Proceedings of the Sixth International Heat Transfer Conference*, Vol. 1, pages 239-243, Toronto, Canada, August 7-11, 1978.
- [42] P. Savic and G.T. Boulton. The fluid flow associated with the impact of liquid drops with solid surfaces. *Proceedings of Heat Transfer Fluid Mechanics Institution*, 43-84, 1957.
- [43] S.E. Hinkle. Water drop kinetic energy and momentum measurement considerations. *Applied Engineering in Agriculture*, 5(3):386–391, 1989. doi: [10.13031/2013.26532](https://doi.org/10.13031/2013.26532).
- [44] C.D. Stow and R.D. Stainer. The physical products of a splashing water drop. *Journal of Meteorological Society of Japan*, 55(5):518–532, 1977.
- [45] Z. Levin and P.V. Hobbs. Splashing of water drops on solid and wetted surfaces, Hydrodynamics and charge separation. *Philosophical Transactions of the Royal Society A Mathematical, Physical and Engineering Sciences*, 269(1200):555–585, 1971. doi: [10.1098/rsta.1971.0052](https://doi.org/10.1098/rsta.1971.0052).
- [46] C.D. Stow and M.G. Hadfield. An experimental investigation of fluid flow resulting from the impact of a water drop with an unyielding dry surface. *Proceedings of the Royal Society A: Mathematical, Physical and Engineering Sciences*, 37(1755):419–441, 1981. doi: [10.1098/rspa.1981.0002](https://doi.org/10.1098/rspa.1981.0002).
- [47] C. Mundo, M. Sommerfeld, and C. Tropea. Droplet-wall collisions: Experimental studies of the deformation and breakup process. *International Journal of Multiphase Flow*, 21(2):151–173, 1995. doi: [10.1016/0301-9322\(94\)00069-V](https://doi.org/10.1016/0301-9322(94)00069-V).
- [48] M. Bussmann, S. Chandra, and J. Mostaghimi. Modeling the splash of a droplet impacting a solid surface. *Physics of Fluids*, 12(12):3121–3132, 2000. doi: [10.1063/1.1321258](https://doi.org/10.1063/1.1321258).
- [49] L. Xu, W.W. Zhang, and S.R. Nagel. Drop splashing on a dry smooth surface. *Physical Review Letters*, 94(18):184505, 2005. doi: [10.1103/PhysRevLett.94.184505](https://doi.org/10.1103/PhysRevLett.94.184505).
- [50] B.T. Helenbrook and C.F. Edwards. Quasi-steady deformation and drag of uncontaminated liquid drops. *International Journal of Multiphase Flow*, 28(10):1631–1657, 2002. doi: [10.1016/S0301-9322\(02\)00073-3](https://doi.org/10.1016/S0301-9322(02)00073-3).
- [51] J.Q. Feng. A deformable liquid drop falling through a quiescent gas at terminal velocity. *Journal of Fluid Mechanics*, 658:438–462, 2010. doi: [10.1017/S0022112010001825](https://doi.org/10.1017/S0022112010001825).
- [52] J.Q. Feng and K.V. Beard. Raindrop shape determined by computing steady axisymmetric solutions for Navier-Stokes equations. *Atmospheric Research*, 101(1–2):480–491, 2011. doi: [10.1016/j.atmosres.2011.04.012](https://doi.org/10.1016/j.atmosres.2011.04.012).
- [53] J. Han and G. Tryggvason. Secondary breakup of axisymmetric liquid drops. I. Acceleration by a constant body force. *Physics of Fluids*, 11(12):3650–3667, 1999. doi: [10.1063/1.870229](https://doi.org/10.1063/1.870229).
- [54] J. Han and G. Tryggvason. Secondary breakup of a axisymmetric liquid drops. II. Impulsive acceleration. *Physics of Fluids*, 13(6):1554–1565, 2001. doi: [10.1063/1.1370389](https://doi.org/10.1063/1.1370389).

- [55] P. Khare and V. Yang. Breakup of non-Newtonian liquid droplets. *44th AIAA Fluid Dynamics Conference*, Atlanta, USA, 16-20 June 2014. doi: [10.2514/6.2014-2919](https://doi.org/10.2514/6.2014-2919).
- [56] M. Sussman and E.G. Puckett. A Coupled level set and volume-of-fluid method for computing 3D and axisymmetric incompressible two-phase flows. *Journal of Computational Physics*, 162(2):301–337, 2000. doi: [10.1006/jcph.2000.6537](https://doi.org/10.1006/jcph.2000.6537).
- [57] R. Scardovelli and S. Zaleski. Direct numerical simulation of free-surface and interfacial flow. *Annual Review of Fluid Mechanics*, 31:567–603, 1999. doi: [10.1146/annurev.fluid.31.1.567](https://doi.org/10.1146/annurev.fluid.31.1.567).
- [58] S. Shin and D. Juric. Simulation of droplet impact on a solid surface using the level contour reconstruction method. *Journal of Mechanical Science and Technology*, 23:2434–2443, 2009. doi: [10.1007/s12206-009-0621-z](https://doi.org/10.1007/s12206-009-0621-z).
- [59] M. García Pérez and E. Vakkilainen. A comparison of turbulence models and two and three dimensional meshes for unsteady CFD ash deposition tools. *Fuel*, 237:806–811, 2019. doi: [10.1016/j.fuel.2018.10.066](https://doi.org/10.1016/j.fuel.2018.10.066).
- [60] M. Mezhericher, A. Levy, and I. Borde. Modeling of droplet drying in spray chambers using 2D and 3D computational fluid dynamics. *Drying Technology*, 27(3):359–370, 2009. doi: [10.1080/07373930802682940](https://doi.org/10.1080/07373930802682940).
- [61] S. Afkhami and M. Bussmann. Height functions for applying contact angles to 2D VOF simulations. *International Journal for Numerical Methods in Fluids*, 57(4):453-472, 2008. doi: [10.1002/flid.1651](https://doi.org/10.1002/flid.1651).
- [62] J. Zheng, J. Wang, Y. Yu, and T. Chen. Hydrodynamics of droplet impingement on a thin horizontal wire. *Mathematical Problems in Engineering*, 2018:9818494, 2018. doi: [10.1155/2018/9818494](https://doi.org/10.1155/2018/9818494).
- [63] J. Thalackottore Jose and J.F. Dunne. Numerical simulation of single-droplet dynamics, vaporization, and heat transfer from impingement onto static and vibrating surfaces. *Fluids*, 5(4):188, 2020. doi: [10.3390/fluids5040188](https://doi.org/10.3390/fluids5040188).
- [64] H. Liu. *Science and Engineering of Droplets: Fundamentals and Applications*. Noyes Publications, USA, 1999.